JACS
JOURNAL OF THE AMERICAN CHEMICAL SOCIETY
pubs.acs.org/JACS
Article

Deciphering the Synchronization of Alternating Current Frequency with the Nickel Catalytic Cycle in Selective C−N Cross-Coupling

Atanu Hazra, Marisa Organiscak, and Long Luo*

Cite This: https://doi.org/10.1021/jacs.5c13155
Read Online
ACCESS | Metrics & More | Article Recommendations | Supporting Information

ABSTRACT: Alternating current (AC) electrolysis offers a promising strategy for modulating redox states in metal-catalyzed reactions, yet its mechanistic basis remains poorly understood. Here, we uncover how AC frequency synchronizes with key steps in a Ni-catalyzed cross-coupling cycle to control product selectivity between C−N and C−C coupling. We show that optimal C−N selectivity arises from minimizing the exposure of a key intermediate, $Ni^{II}(Ar)Br$, to reducing conditions that otherwise promote off-cycle Ni^{I} species and undesired C−C homocoupling. By developing a simple cyclic voltammetry-based method, we accurately predict the optimal AC frequency across diverse aryl bromides and amines, eliminating the need for time-consuming trial-and-error reaction optimization. The predicted values align well with experimentally determined frequencies, validating the approach. This work establishes a mechanistic foundation for integrating AC waveform control into metal catalysis and highlights its potential for advancing selective electrochemical transformations in synthetic and medicinal chemistry.

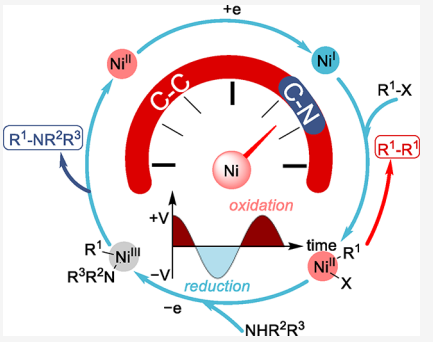

INTRODUCTION

Metal-catalyzed cross-coupling reactions are powerful tools for constructing complex organic molecules and play a pivotal role in modern drug discovery.[1−4] Figure 1a(i) illustrates a general schematic of a classical metal-catalyzed cross-coupling reaction, which typically begins with the metal catalyst in its oxidized form (M_{ox}). Upon reduction ($+ne^-$), the active reduced species (M_{red}) is generated. This species undergoes oxidative addition with an electrophile, such as an aryl or alkyl halide, to form a metal−aryl/alkyl−halide complex. This is followed by transmetalation, in which the halide is replaced by a nucleophile or another functional group. Finally, reductive elimination releases the cross-coupled product and regenerates the catalyst for the next catalytic cycle.[5−10]

Each step in such a catalytic cycle proceeds at its own characteristic rate, requiring a specific amount of time (t_1, t_2, etc.) to complete before the next step can occur. The overall efficiency of the cycle is governed by rate matching among these steps—mismatches can lead to the formation of inactive off-cycle species or undesired side products.[11−14] For instance, in a Pd-catalyzed cross-coupling cycle, if the reduced form of palladium (Pd^0) is not promptly engaged in the subsequent catalytic step, it may aggregate to form Pd nanoparticles instead of progressing through the intended reaction sequence.[15−17] Traditional strategies to address this challenge include ligand design and the use of chemical additives.[18]

Alternating current (AC) electrolysis, which applies an oscillating voltage to drive redox events, offers an alternative to traditional chemical-based strategies for controlling rate matching within catalytic cycles. As illustrated in Figure 1a(ii), the key concept involves superimposing a dynamic redox environment provided by AC electrolysis onto the metal catalytic cycle to modulate the speciation of metal complexes in real time. This enables the rate tuning of individual steps within the cycle. This concept of synchronizing AC electrolysis with metal catalysis has recently garnered considerable attention. For example, Lei and co-workers have developed various C−H functionalization methods while addressing challenges such as metal catalyst deposition.[19] Semenov's group demonstrated that AC can improve both the yield and scalability of Ni-catalyzed cross-coupling transformations.[20] De Bon et al. reported that AC electrolysis improved the efficiency and controllability in Cu-catalyzed electrochemically mediated atom transfer radical polymerization.[21] Their work highlights how the dynamic redox environment of AC electrolysis can overcome key limitations of conventional methods.

Despite recent advances, a comprehensive and quantitative mechanistic understanding of metal-catalyzed reactions under AC electrolysis conditions remains limited. Critical insight into how the dynamic redox environment influences the catalytic process is still lacking, which is essential for the informed development of future AC-enabled catalytic transformations.

Received: July 31, 2025
Revised: September 3, 2025
Accepted: September 4, 2025

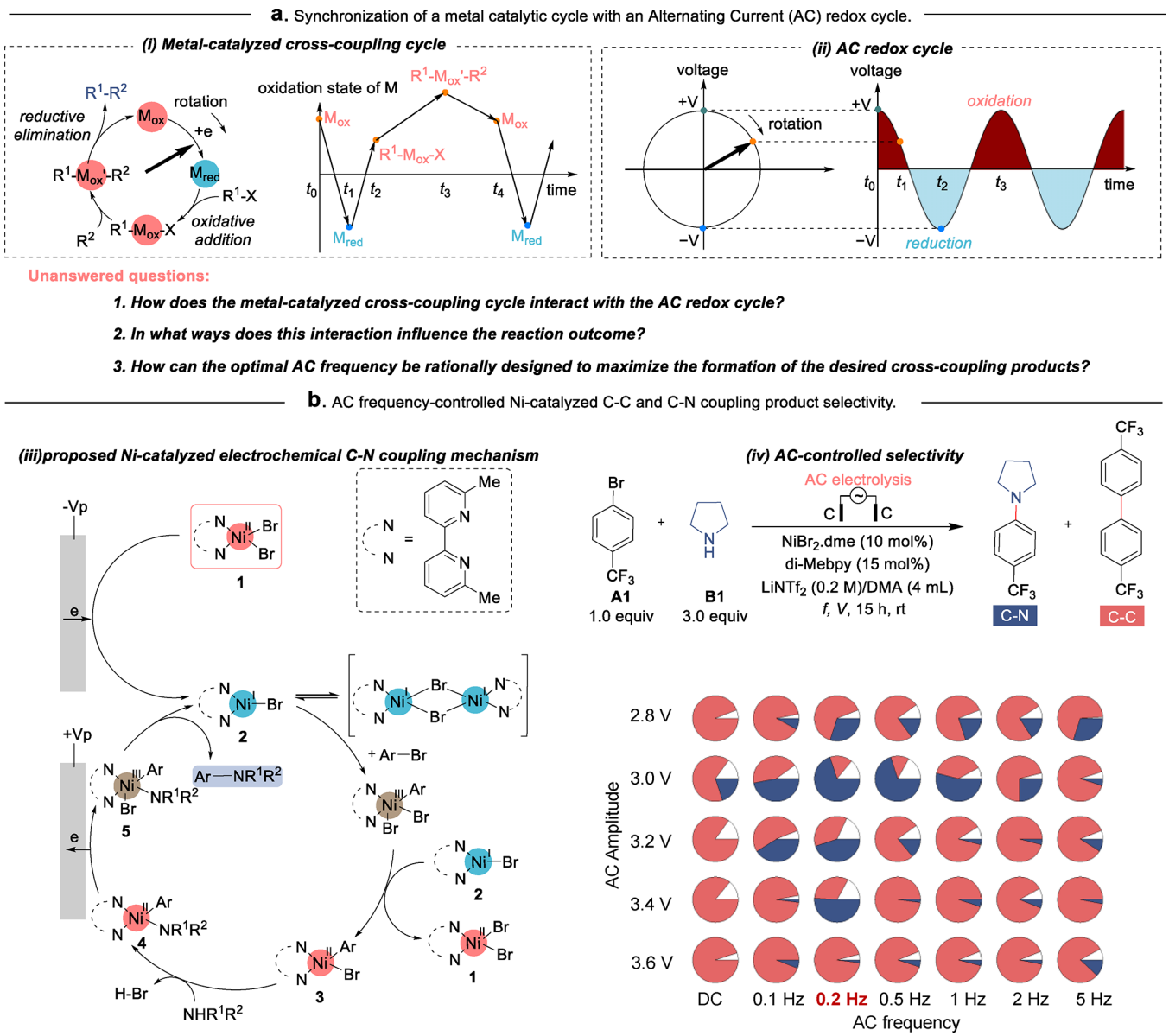

Figure 1. (a) Schematic illustration of synchronizing a metal-catalyzed cross-coupling cycle with an alternating current (AC) redox cycle. (i) The cross-coupling catalytic cycle involves periodic transitions between oxidized (M_{ox}) and reduced (M_{red}) metal states, enabling bond formation (R^1–R^2). (ii) The AC redox cycle modulates these oxidation states temporally, introducing synchronized redox control through applied AC waveforms (sine wave). (b) AC frequency-dependent product selectivity in AC-enhanced Ni-catalyzed C–N cross-coupling reactions. (iii) The proposed mechanism for the electrochemical Ni-catalyzed C–N cross-coupling reaction. (iv) The AC frequency modulates the selectivity between C–N and C–C coupling products. The pie chart matrix displays product distribution (C–N in blue, C–C in red) at varying sine waveform frequencies and amplitudes, with the highest C–N selectivity at 0.2 Hz and 3.0 V.

Several key questions remain unanswered: How does a metal-based catalytic cycle interact with the AC redox cycle? In what ways does this interaction affect the reaction outcome? And how can the optimal AC frequency be rationally designed to favor formation of the desired product?

In this study, we investigated a Ni-catalyzed model reaction as illustrated in Figure 1b, which exhibits AC frequency-dependent selectivity between C–N cross-coupling and C–C homocoupling, to address the above questions. Our results show that enhanced selectivity toward the C–N cross-coupling product at an optimal AC frequency arises from minimizing the exposure of a key intermediate, $Ni^{II}(Ar)Br$ (**3**), to reducing conditions. Prolonged reduction promotes the formation of an off-cycle Ni^{I} species that triggers the undesired reductive C–C homocoupling pathway. The formation rate of intermediate **3** is governed by the oxidative addition of ArBr to the $Ni^{I}Br$ species (**2**) to form a short-lived Ni^{III} species, followed by reaction with **2**,[22] which itself originates from cathodic reduction of $Ni^{II}Br_2$ (**1**). Therefore, the timing of **3** formation is highly dependent on the identity of the ArBr electrophile but largely independent of the amine coupling partner (NHR_1R_2), as supported by our experimental data. Furthermore, we developed a convenient electroanalytical method based on cyclic voltammetry (CV) to predict the ideal AC frequency for various ArBr substrates, thereby circumventing the need for time-consuming trial-and-error reaction condition screening. This advancement provides a mechanistic foundation for synchronizing AC frequency with a

https://doi.org/10.1021/jacs.5c13155
J. Am. Chem. Soc. XXXX, XXX, XXX−XXX

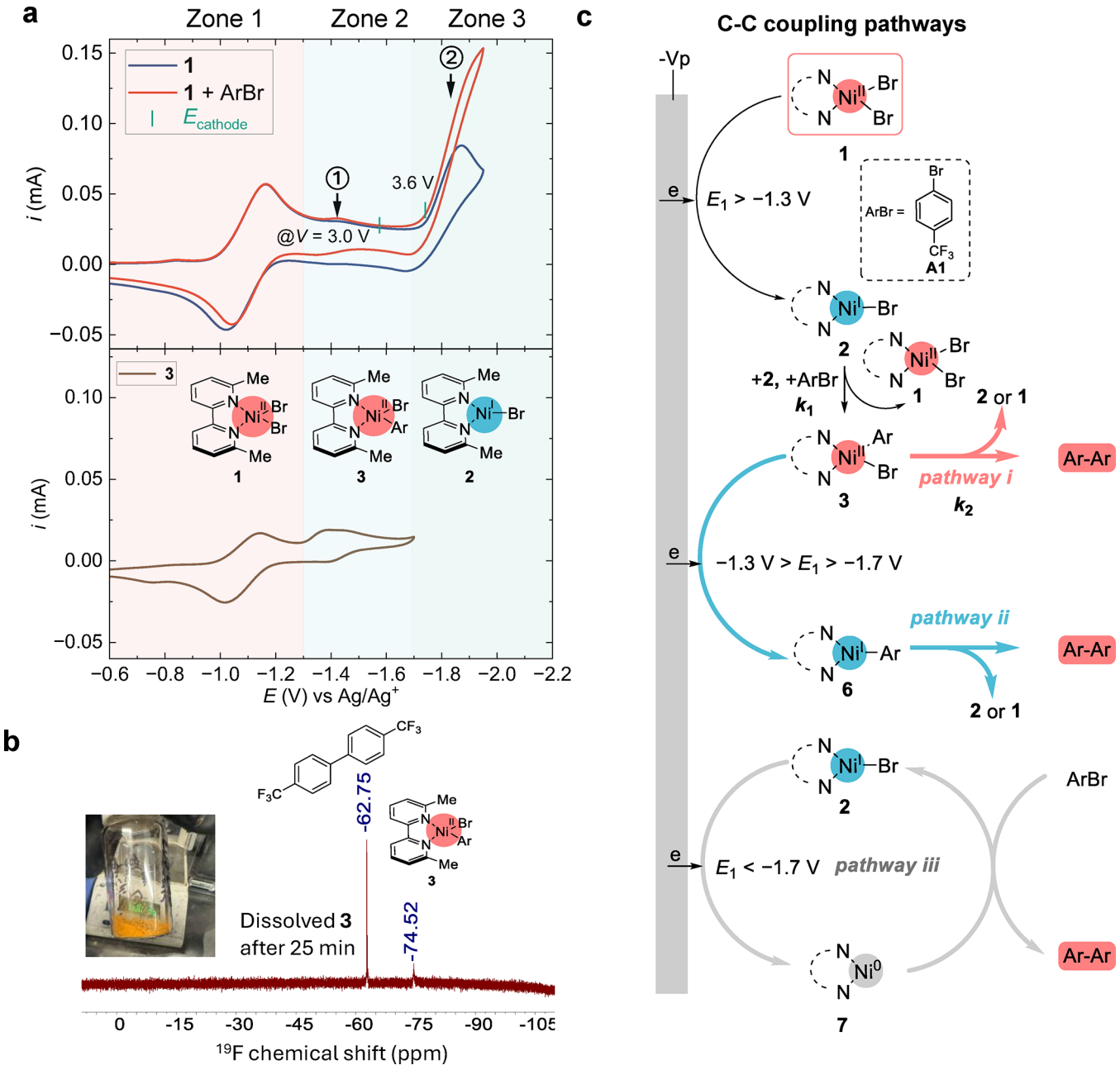

Figure 2. (a) CVs of compound **1** recorded in the presence and absence of **A1** in DMA with 0.1 M $LiNTf_2$ at a scan rate of 0.1 V/s, illustrating the cathodic reduction potentials across different amplitudes. A CV of synthesized compound **3** under identical conditions is also shown. (b) ^{19}F NMR spectrum of the synthesized compound **3** after 25 min in CD_2Cl_2, showing residual **3** along with the C−C coupling product as the major species. (c) Proposed mechanism for C−C coupling under cathodic reduction conditions, highlighting that intermediates **3**, **6**, and **7** lead to the C−C homocoupling product formation (for details, see Figure S25).

metal catalytic cycle, enabling rational design of selective electrochemical transformations.

RESULTS AND DISCUSSION

AC Frequency-Controlled C−N vs C−C Coupling. Electrochemical Ni-catalyzed C−N coupling reactions were first developed by the Baran group, who employed Ni^{II}(bipyridine) catalysts under direct current (DC) electrolysis conditions.[23] They later expanded this methodology to enable the amination of amino acids, oligopeptides, and nucleoside nucleophiles.[24] The proposed reaction mechanism, illustrated in Figure 1b(iii), involves cathodic reduction of $Ni^{II}Br_2$ (**1**) to generate $Ni^{I}Br$ species (**2**), which undergoes oxidative addition with ArBr to form Ni^{II}(Ar)Br (**3**). This intermediate then engages in ligand exchange with an amine (NHR^1R^2) to yield Ni^{II}(Ar)(NR^1R^2) (**4**). Oxidation of **4** at the anode generates a high-valent Ni^{III} species (**5**), which undergoes reductive elimination to furnish the C−N coupling product (Ar−NR^1R^2) and regenerate the active $Ni^{I}Br$ catalyst (**2**). In follow-up work, Semenov and co-workers demonstrated that applying AC electrolysis improved selectivity toward the C−N coupling product.[20] However, the mechanistic basis for this enhancement remained unclear. Notably, both the Baran and Semenov protocols used LiBr as the electrolyte, which was later shown by the Liu group to participate directly in the catalytic cycle.[25] Specifically, the oxidation of intermediate **4** to **5** does

https://doi.org/10.1021/jacs.5c13155
J. Am. Chem. Soc. XXXX, XXX, XXX−XXX

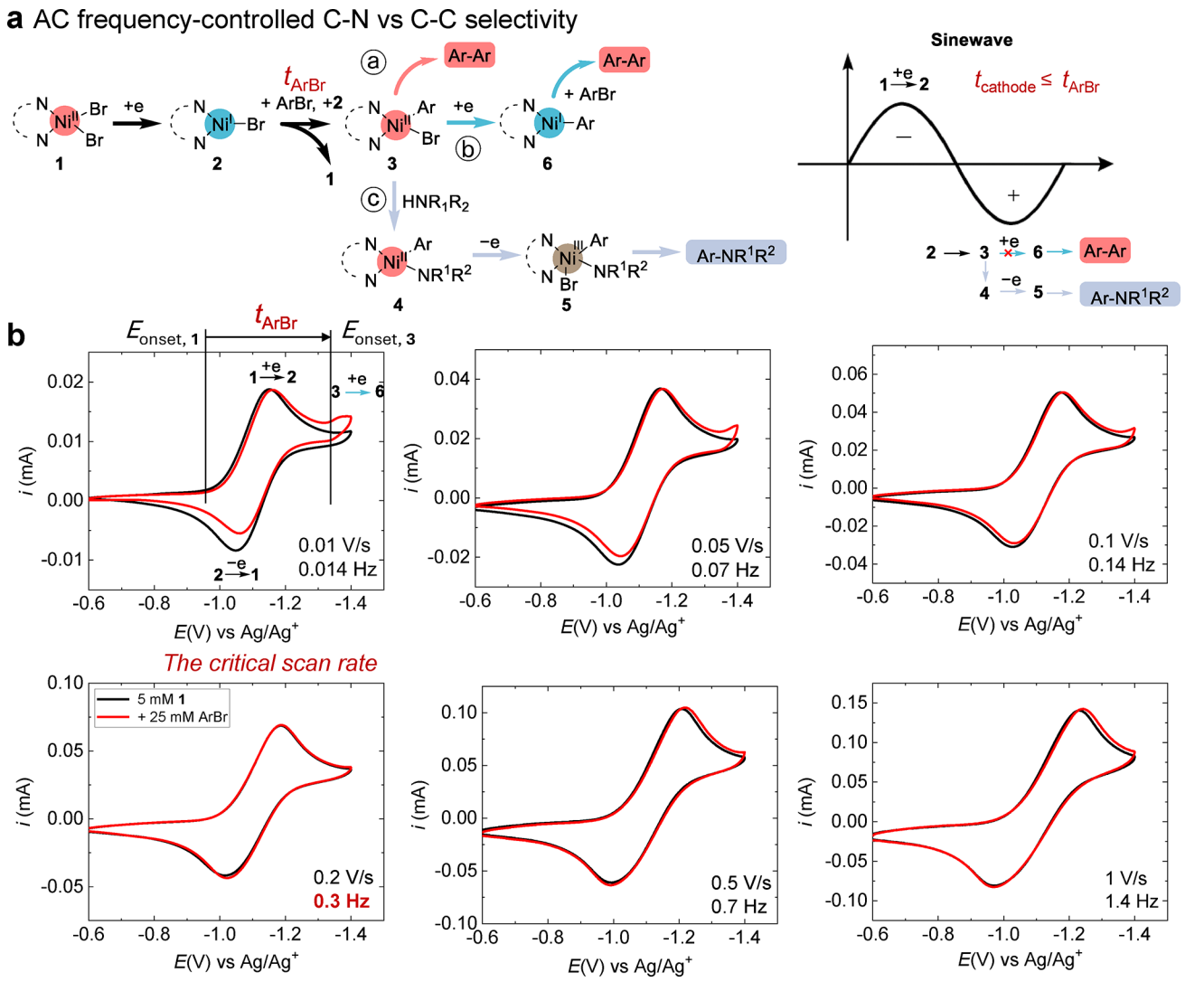

Figure 3. (a) Left: Reaction pathways governing C−N versus C−C selectivity. Complex **3** serves as a key branching point in the mechanistic network. Right: Temporal alignment between the optimal AC waveform (sine wave) and the key reaction steps. At the optimal frequency for selective C−N coupling, the cathodic half-wave duration ($t_{cathode}$) should become less than or equal to the oxidative addition time (t_{ArBr}). (b) CVs of **1** in the absence (black trace) and presence (red trace) of ArBr at various scan rates ranging from 0.01 to 1 V/s with their corresponding equivalent AC frequency. $E_{onset,1}$ and $E_{onset,3}$ are the onset potentials for the **1** → **2** reduction and the **3** → **6** reduction. t_{ArBr} is estimated from the time that it takes to scan from $E_{onset,1}$ to $E_{onset,3}$ at the critical scan rate of 0.2 V/s when the two CVs completely overlap.

not proceed via direct anodic oxidation, but instead occurs via chemical oxidation by molecular bromine (Br_2), generated in situ from the anodic oxidation of bromide ions (Br^-).

The reversible redox chemistry of the Br^-/Br_2 couple complicates the mechanistic analysis of the impact of AC electrolysis on the Ni-catalyzed coupling reaction. To minimize this confounding factor, we replaced the LiBr electrolyte with the redox-inert lithium bis(trifluoromethane-sulfonyl) imide ($LiNTf_2$). Additionally, we employed 6,6′-dimethyl-2,2′-bipyridine (di-Mebpy) as the ligand, whose corresponding Ni^{II} complex exhibits highly reversible redox behavior under electrochemical conditions.[26] This substitution helps minimize side reactions associated with the decomposition of Ni complexes during redox cycling, allowing for a more controlled and interpretable investigation of AC frequency effects.

Using the modified reaction conditions, we systematically evaluated product selectivity as a function of AC frequency and amplitude (f = 0−5 Hz; V = 2.8−3.6 V, Figures S1 and S2). As shown in Figure 1b(iv), the selectivity between C−N (blue) and C−C (red) coupling products is strongly dependent on both f and V. Optimal C−N selectivity is observed at a specific frequency of 0.2 Hz across most voltage values. However, the highest yield of the C−N coupling product is achieved at an amplitude of 3.0 V; deviations from this value, either above or below, lead to a marked decrease in C−N product formation. These trends are consistent with previous observations by Semenov,[20] supporting the conclusion that AC-controlled selectivity arises from intrinsic features of the Ni-catalytic cycle rather than from Br^-/Br_2 redox chemistry. The near-zero yield observed under our DC conditions, significantly lower than that reported under Semenov's DC conditions, is because the intermediate **4** could not be electrochemically oxidized to **5** efficiently in the absence of Br^-/Br_2 redox chemistry. We also confirmed the importance of anodic oxidation of **4** to **5** in the C−N coupling reaction by running a divided cell experiment, in which only the C−C homocoupling product was found (Figure S3).

https://doi.org/10.1021/jacs.5c13155
J. Am. Chem. Soc. XXXX, XXX, XXX−XXX

Identifying the C−C Homocoupling Pathways. To quantitatively understand the effect of AC electrolysis on the C−N vs C−C coupling selectivity, we began by identifying the C−C coupling pathways in this Ni-catalyzed system using CV analysis. The top panel of Figure 2a shows the CV of the Ni catalyst, Ni^{II}(di-Mebpy)Br_2 (**1**), with and without the model ArBr, 4-bromo-1-(trifluoromethyl) benzene (**A1**). The CV of **1** alone (blue trace) displays a pair of reversible redox peaks in Zone 1 (-0.6 V > E > -1.3 V), corresponding to the Ni^{II}/Ni^{I} redox couple (i.e., **1**/**2**), and a pair of quasireversible peaks in Zone 3 ($E < -1.7$ V), attributed to the further reduction of Ni^{I} species, **2**, to a Ni^{0} species, **7**.[26] Note that the electrode potentials reported herein are referenced to Ag/10 mM Ag^{+} unless otherwise noted. Also, the reduction of Ni^{II} to Ni^{I} in Zone 1 could proceed via a first reduction to a Ni^{0} species with subsequent generation of Ni^{I} by rapid comproportionation with Ni^{II}.[22,27]

Upon addition of ArBr (**A1**), two notable changes were observed in the CV (red vs blue curve in Figure 2a): ① the appearance of a small peak at approximately −1.4 V and ② a pronounced increase in current in Zone 3, accompanied by the disappearance of the anodic return wave.

For observation ①, we hypothesized that the new peak at ∼−1.4 V arises from the reduction of Ni^{II} complex **3**, which forms via oxidative addition of ArBr to the Ni^{I} species **2**. To test this hypothesis, we synthesized complex **3** using a reported procedure (Figure S4).[28] The photograph of **3** is shown in the inset of Figure 2b. The CV of **3**, shown in the lower panel of Figure 2a, displays two distinct peaks: the first corresponds to the **1**/**2** redox couple, consistent with the upper CV trace, while the second is assigned to the reduction of complex **3** itself. Note that the presence of the **1**/**2** redox feature in the CV of **3** is attributed to the spontaneous decomposition of **3**, which generates complex **1** and forms the C−C homocoupling product.[28] This decomposition is supported by the ^{19}F NMR spectrum of **3** in Figure 2b, recorded 25 min after dissolving the solid in CD_2Cl_2.

For observation ②, the transition from a peak shape to a sigmoidal-shape-like wave is characteristic of a catalytic electron-transfer process, in which electrochemical reduction or oxidation generates a species that undergoes a subsequent chemical transformation, regenerating the original redox-active species—commonly referred to as an EC′ mechanism.[29] This CV feature indicates that the Ni^{0} species **7**, formed by the reduction of **2**, reacts with ArBr to regenerate **2**, thereby catalyzing the electrochemical reduction of ArBr.

To further interpret these CV results, we correlated them with the synthetic outcomes observed at different AC amplitudes. At V = 3.6 V, the cathodic potential ($E_{cathode}$) was measured to be −1.74 V vs Ag/Ag^{+} (Figure S9), corresponding to Zone 3 in Figure 2a. Under these conditions, the C−C homocoupling product was the predominant product, indicating that the EC′ reaction between **2** and ArBr primarily leads to homocoupling rather than the C−N cross-coupling. When V decreased to the optimal value of 3.0 V, $E_{cathode}$ was found to be −1.58 V, corresponding to Zone 2, insufficient to generate Ni^{0} but enough to reduce **3** to generate a Ni^{I} species, **6**. Compound **6** has previously been proposed to form the C−C homocoupling product via two possible mechanisms: (i) a second oxidative addition with ArBr, forming a $Ni^{III}(Ar)_2Br$ intermediate that subsequently undergoes reductive elimination,[30] or (ii) transmetalation with Ni^{II}(Ar)Br species to form $Ni^{II}(Ar)_2$ intermediates.[31]

Taken together, we have identified three distinct C−C homocoupling pathways under AC electrolysis conditions, as summarized in Figure 2c: (i)the chemical decomposition of the Ni^{II} complex **3**. (ii) the reactions of the Ni^{I} complex **6** with ArBr, and (iii) the EC′ reaction between species **2** and ArBr. Under optimal AC electrolysis conditions for selective C−N coupling (i.e., 3.0 V and 0.2 Hz), only the first two pathways could occur.

Origin of AC Frequency-Dependent Product Selectivity. By integrating the identified C−C and C−N coupling pathways, we identified the Ni^{II} complex, **3**, as a key branching node in the mechanistic network shown in Figure 3a. Specifically, the selectivity between C−C and C−N products is governed by three possible fates of **3**: ⓐ chemical decomposition, ⓑ further reduction to **6**, and ⓒ transmetalation with the amine.

The rates of pathways ⓐ and ⓒ are determined by the intrinsic chemical properties of **3** and the amine, and are largely independent of the electrochemical conditions. In contrast, the electrochemical step ⓑ can be modulated by the applied AC frequency. By avoiding a reducing environment that promotes the formation of **6**, AC electrolysis can suppress the C−C homocoupling pathway ⓑ and enhance selectivity for the C−N product. Therefore, the optimal AC frequency is one that minimizes the exposure of **3** to reductive potentials, as illustrated in the right panel of Figure 3a. The duration of the cathodic half-wave ($t_{cathode}$) should be shorter than the time scale of the oxidative addition of ArBr to the Ni^{I} species **2** (t_{ArBr}). In this way, compound **3** will only form in the anodic half-wave and thus will not be reduced to **6** and trigger the C−C homocoupling pathway ⓑ.

To estimate t_{ArBr}, we performed CV analysis of the Ni^{II}/Ni^{I} redox couple in the absence (black trace) and presence (red trace) of ArBr at various scan rates (v) ranging from 0.01 to 1 V/s (Figure 3b). At the slowest v = 0.01 V/s, we clearly observed the initial reduction of **1** to **2**, as well as an increase in current corresponding to the conversion of **3** to **6** upon addition of ArBr (red trace). Additionally, there is a decrease in current for the **2** to **1** transition in the reverse scan. As we increased the scan rates, thereby reducing the time available for oxidative addition, the CV traces with and without ArBr (black and red) began to overlap. At v = 0.2 V/s, we observed no evidence of oxidative addition—this represents the critical threshold, from which t_{ArBr} can be extracted as follows.

First, we identified the onset potentials for the **1** → **2** reduction ($E_{onset,1} \approx -0.95$ V) and the **3** → **6** reduction ($E_{onset,3} \approx -1.3$ V) from the CV. Scanning the electrode potential from $E_{onset,1}$ to $E_{onset,3}$ can be considered a generation-and-collection experiment: species **2** is first generated from **1** at $E_{onset,1}$, and the product **3**, formed via oxidative addition between **2** and ArBr, is collected at $E_{onset,3}$. At different scan rates, the reaction between **2** and ArBr is allowed to proceed for varying durations. At a critical scan rate of 0.2 V/s, no product **3** was collected, indicating that the reaction time with ArBr (t_{ArBr}) becomes longer than the time it takes to scan from $E_{onset,1}$ to $E_{onset,3}$ ($|E_{onset,1} - E_{onset,3}|/v$ = 1.75 s). In other words, using an AC waveform with a cathodic half-wave duration ($t_{cathode}$) of 1.75 s (equivalent to f = 0.3 Hz, see Figure S7) would minimize the exposure of **3** to the reducing environment, thereby yielding the highest selectivity for C−N cross-coupling. The optimal frequency predicted from CV analysis (f_{pred} = 0.3 Hz) is in good agreement with the experimentally determined optimal frequency (f_{exp} = 0.2 Hz; Figure 1b(iv)). Note that applying frequencies higher than f_{pred} does not necessarily maintain high

https://doi.org/10.1021/jacs.5c13155
J. Am. Chem. Soc. XXXX, XXX, XXX−XXX

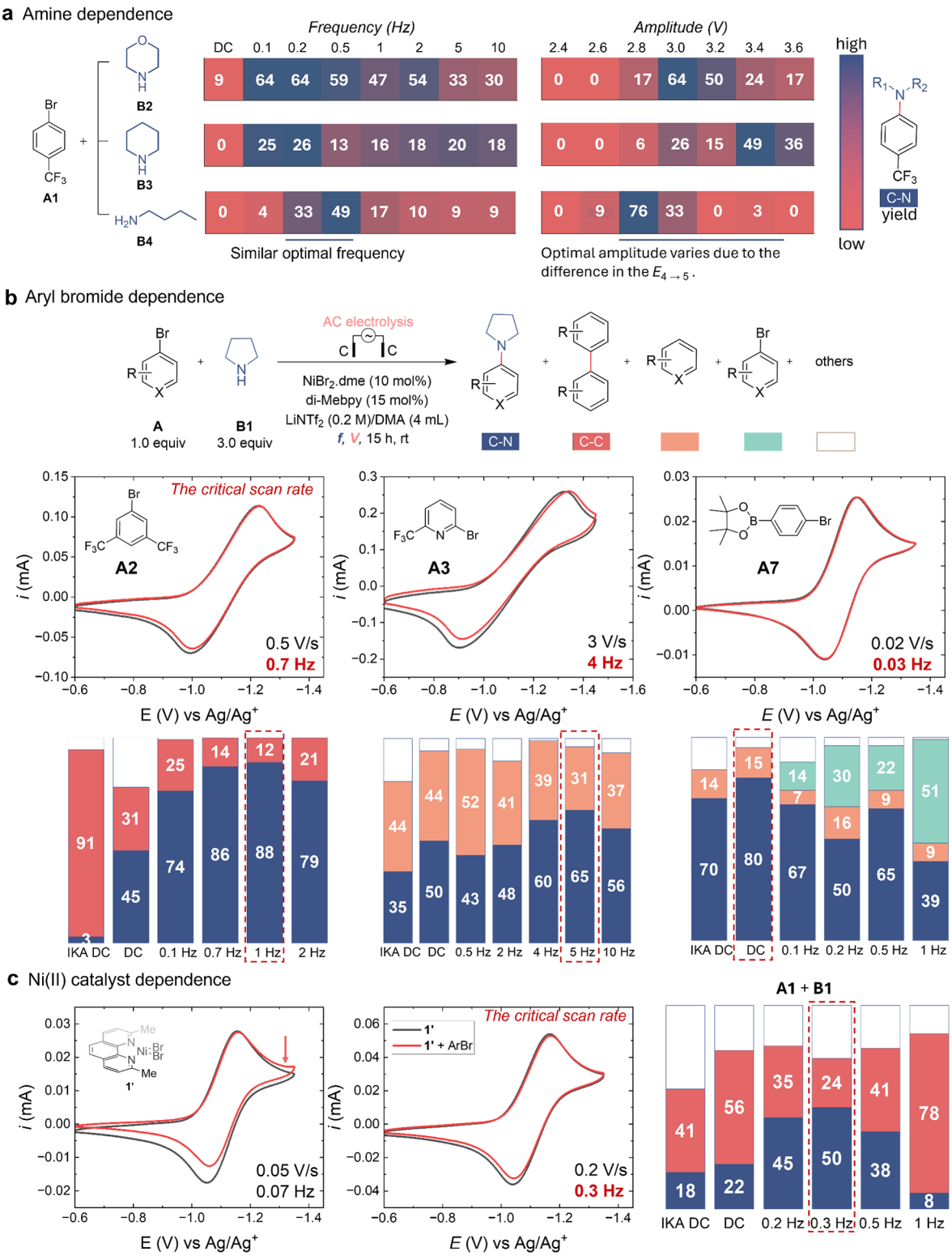

Figure 4. (a) Heatmaps depicting product distributions from the reaction between **A1** and various amine coupling partners **B2**, **B3**, and **B4** under AC electrolysis reveal a consistent optimal frequency range of 0.2−0.5 Hz (amplitude was fixed at 3.0 V) with optimal amplitudes between 2.8 and 3.4 V (frequency was kept at 0.2 Hz). (b) CVs of Ni catalyst **1** with (red) and without (black) three representative aryl bromides—**A2**, **A3**, and **A7**—measured at their corresponding critical scan rates (0.7, 4, and 0.03 Hz, respectively). Predicted optimal frequencies (highlighted in red) align well with experimentally determined values (indicated by dashed red boxes). (c) Critical scan rate of 0.3 Hz was identified for Ni^{II} catalyst **1′** bearing a neocuproine ligand, showing strong agreement between the predicted optimal frequency and the experimental one.

C−N coupling product selectivity, possibly due to a "carryover effect." At very high frequencies, **1** is first reduced to **2** during the cathodic half-wave. Upon switching to the anodic half-wave, a portion of **2** undergoes oxidative addition with Ar−Br to form **3**. However, if **3** cannot efficiently convert to **4** within the shortened anodic time window and is instead carried over into

https://doi.org/10.1021/jacs.5c13155
J. Am. Chem. Soc. XXXX, XXX, XXX−XXX

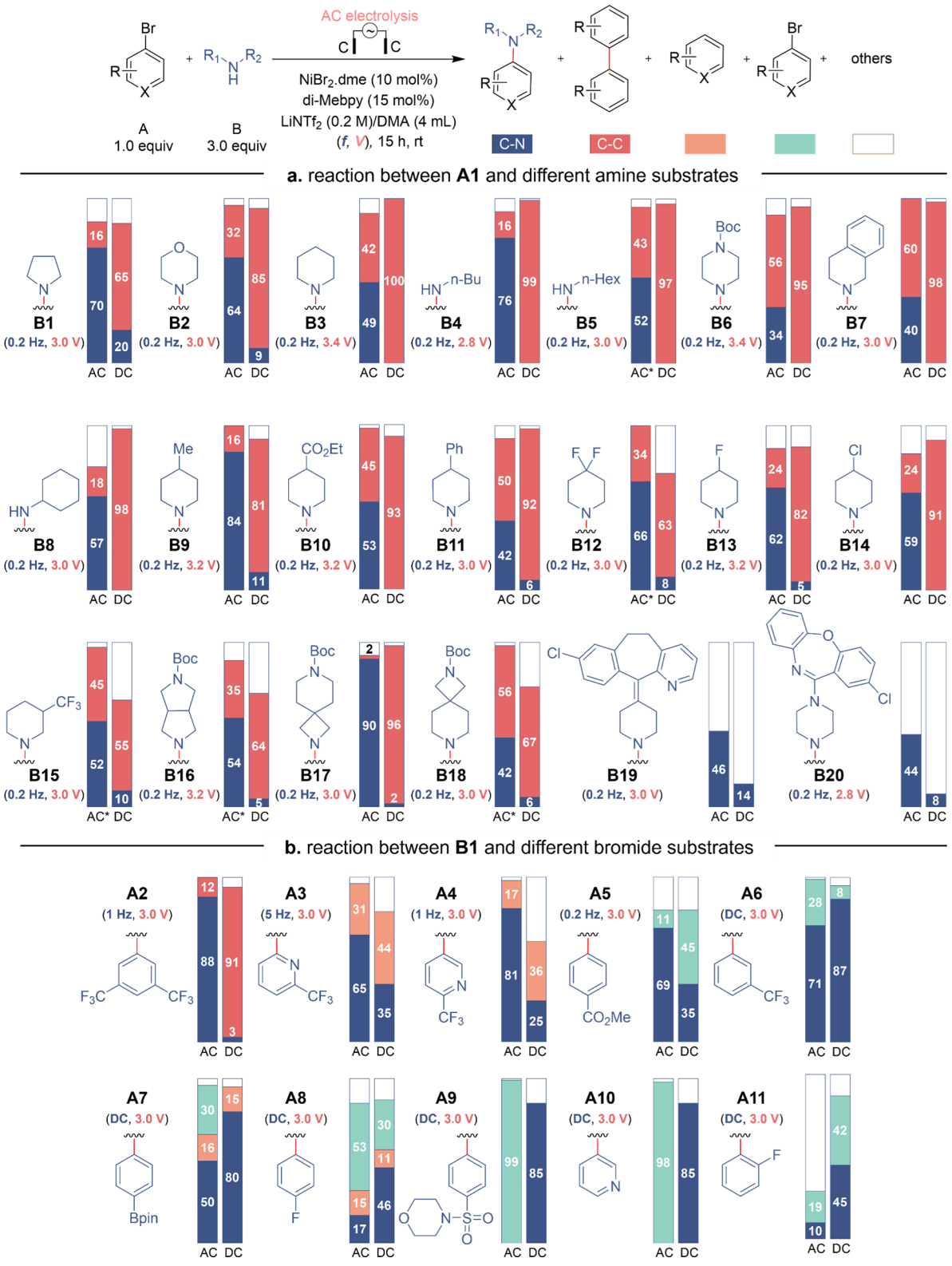

Figure 5. Substrate scope and product selectivity comparison between AC and DC electrolysis for C−N and C−C coupling from (a) various amines and (b) aryl bromides. Product yields for C−N and C−C coupling were determined by ^{19}F NMR using hexafluorobenzene as an internal standard, except **A5**, **A7**, **A9**, and **A10**, whose product yields were determined by ^{1}H NMR using 1,3,5-trimethoxybenzene as the internal standard. *The di^{t}Bubpy ligand was used to improve the C−N coupling yields (for details, see Figure S11). The AC results for **A6**−**A11** were obtained from 0.2 Hz, and their corresponding DC results were collected using the home-built electrochemical cell.

the subsequent cathodic pulse, where it is reduced to **6**. This pathway ultimately favors Ar−Ar homocoupling as the predominant reaction outcome.

Effects of Amines and Aryl Bromides on the Optimal *f*.

The close agreement between f_{pred} and f_{exp} for the Ni-catalyzed C−N cross-coupling reaction between **A1** and **B2** motivated us

https://doi.org/10.1021/jacs.5c13155
J. Am. Chem. Soc. XXXX, XXX, XXX−XXX

to test this CV-based prediction on different amines and aryl bromides. Based on the mechanistic analysis of C−N vs C−C selectivity shown in Figure 3a, the optimal AC frequency is expected to be determined solely by the aryl bromide and independent of the amine component.

To validate our analysis, we first conducted experiments using different amines, **B2**, **B3**, and **B4**, while keeping **A1** constant. In all cases, the f_{exp} for C−N cross-coupling was similar, around 0.2 to 0.5 Hz, which aligns well with f_{pred} of 0.3 Hz (Figure 4a). However, the optimal AC amplitude significantly varied between 2.8 and 3.4 V. This variation is likely due to differences in the oxidation potential of the $Ni^{II}(Ar)(NR_1R_2)$ complex (**4**) to the corresponding $Ni^{III}(Ar)(NR_1R_2)Br$ species (**5**), rather than direct oxidation of the amines themselves. Supporting this interpretation, amine **B4**, despite having a higher oxidation potential ($E_{peak} \approx +1.16$ V, Figure S6) than **B2** and **B3** ($E_{peak} \approx +0.95$ V), exhibited a lower optimal AC amplitude (2.8 V vs 3.0−3.4 V). However, attempts to synthesize complex **4** for direct measurement of its redox potential were unsuccessful due to the instability of the precursor complex **3.**

On a side note, we would like to point out that **1** can coordinate with an amine substrate to form a Ni^{II}−amine complex.[25] However, we found that the oxidative addition of its reduced Ni^{I} form by **A1** did not show any evidence of undesired reductive pathways (Figure S24) that were found in the behavior of **1** without amine coordination (**3** → **6** in Figure 3a). This suggests that if amine-coordinated **1** were the primary catalytic species, DC electrolysis would have been the most effective condition, and the optimal electrochemical conditions should be strongly amine-dependent—both of which contradict our experimental observations. Moreover, considering that (1) **1** can be regenerated in situ during the catalytic cycle and (2) the amine is electrochemically consumed at the anode near the electrode surface, we think that the pristine **1** is still most likely the primary active catalyst and the reaction proceeds following the reaction scheme in Figure 3a.

Next, we tested three representative aryl bromides while keeping **B1** constant. We collected CVs for **A2**, **A3**, and **A7** to determine critical scan rate and their f_{pred} values (Figures 4b and S12, S13, S17). In parallel, f_{exp} was determined experimentally through conventional reaction optimization, where reactions were performed at various AC frequencies and product selectivity was assessed via crude NMR analysis (Figures 4b and S8).

For substrate **A2**, which contains two $-CF_3$ groups on the phenyl ring and is therefore more electron-withdrawing than **A1**, a faster oxidative addition was observed. The f_{pred} value for **A2** is 0.7 Hz, in excellent agreement with f_{exp} of 0.7−1 Hz that afforded the highest C−N coupling product yield. Similarly, for substrate **A3**, the presence of the highly electronegative pyridyl ring facilitates a significantly faster oxidative addition compared to **A1** or **A2**. The f_{pred} value for **A3** is 4 Hz, which also aligns well with the f_{exp} value of 5 Hz. Interestingly, even though the dominant side product was from debromination rather than C−C homocoupling, the optimal frequency for C−N coupling is still accurately predicted by the CV analysis. This is possibly because the further reduction of the key $Ni^{II}(Ar)Br$ intermediate contributes to the formation of the debromination side product pathway.

For **A7**, its f_{pred} value is 0.03 Hz; however, we observed an optimal C−N coupling yield under DC conditions using our home-built cell. This is likely because the redox environment transition that an AC waveform with low frequencies, such as 0.03 Hz, can be achieved by moving the key reaction intermediates between two electrodes under DC conditions. It is important to note that the result differed between the IKA DC setup (3 mm interelectrode gap) and our DC setup (1 mm gap), as a larger interelectrode gap increases mass transfer time between electrodes and can promote side reactions. Overall, our results show a good agreement between f_{pred} and f_{exp} across these three aryl bromides with varying positions and natures of substituents on the aromatic ring, confirming the predictive power of this simple electrochemical descriptor for identifying the optimal AC frequency for selective C−N coupling.

The rate of oxidative addition is influenced not only by the nature of the aryl bromide but also by the ligand on the Ni catalyst. To test this, we synthesized the $Ni^{II}Br_2$ complex with a neocuproine ligand (**1′**, Figure 4c). CV experiments conducted both in the absence (black trace) and presence (red trace) of aryl bromide **A1** determine f_{pred} = 0.3 Hz (Figures 4c and S22). Consistent with this prediction, f_{exp} for achieving the highest yield of the C−N cross-coupling product was also 0.3 Hz, further validating the accuracy of our frequency prediction methodology. Being able to predict f_{exp} from CV data is particularly valuable, as identifying the optimal frequency empirically is both time-consuming and labor-intensive. Each reaction requires a dedicated power supply and takes nearly 15 h to complete. In contrast, the entire CV analysis would take less than 1 h.

Substrate Scope. Finally, we applied this optimal frequency prediction method to the broader substrate scope and compared the selectivity of C−N vs C−C coupling products between AC and DC electrolysis (Figure 5).

As previously discussed, the optimal AC frequency should be determined solely by the aryl bromide and independent of the amine coupling partner. Therefore, when reacting aryl bromide **A1** with a range of amine coupling partners (**B1**−**B20**), AC electrolysis was performed at a fixed f_{exp} = 0.2 Hz with varying amplitude to maximize the C−N coupling product yields (Figure S11). In contrast, DC electrolysis was conducted using an IKA setup at the same voltage amplitude as the optimal AC condition.

Among the cyclic secondary amines, pyrrolidine (**B1**) afforded the highest C−N coupling product yield (70%), outperforming morpholine (**B2**, 64%) and piperidine (**B3**, 49%). This trend may be attributed to the reduced steric hindrance of the five-membered ring in **B1**. In contrast, DC electrolysis consistently resulted in diminished yields for the C−N coupling product (0−20%) across all cases. Aliphatic primary amines, such as **B4, B5,** and **B8**, also exhibited good yields under AC conditions, with the less sterically hindered **B4** yielding a higher percentage (76%) compared to **B5** (52%) and **B8** (57%). N-Boc piperazine (**B6**) and tetrahydroisoquinoline (**B7**) furnished moderate yields under AC conditions (34 and 40%, respectively), likely due to their electron-withdrawing character, which may impede efficient coordination to the Ni center. Notably, neither substrate yielded a detectable product under DC conditions. The presence of an electron-donating group on the piperidine ring (**B9**) enhanced reactivity, resulting in an excellent yield (84%), whereas electron-withdrawing substituents (**B10**−**B15**) led to more moderate yields (42−66%). The fused five-membered N-heterocycle **B16** provided a 54% yield under AC conditions, in contrast to only 5% under DC conditions. Spirocyclic amines **B17** and **B18** also demonstrated good to excellent yields, with the less sterically hindered four-membered ring in **B17** affording a notably high yield (90%),

https://doi.org/10.1021/jacs.5c13155
J. Am. Chem. Soc. XXXX, XXX, XXX−XXX

compared to **B18** (42%), which features a six-membered ring on the reactive side.

This AC-driven C−N coupling method offers significant potential for the derivatization of amine motifs in bioactive molecules. To demonstrate its applicability, electrochemical N-arylation was conducted on desloratadine (**B19**) and amoxapine (**B20**), affording the desired C−N coupling products in 46 and 44% yield, respectively (Figure 5a). In contrast, under DC conditions, the corresponding products were obtained in yields of only 14 and 8%. In these reactions, the expensive amine was used as the limiting reagent, with five equiv of aryl bromide. The markedly lower yields under DC conditions were attributed to poor selectivity, with most of the aryl bromide diverted to C−C homocoupling byproducts.

The substrate scope was further extended to a series of aryl bromides (**A2**−**A10**, Figure 5b). Like the previously discussed **A2** and **A3** of Figure 4, substrate **A4**, which contains a pyridyl ring, exhibited a rapid oxidative addition with f_{pred} = 1 Hz as determined by CV analysis (Figure S14). f_{exp} that afforded the highest yield of the C−N coupling product (81%) aligned at 1 Hz. Deviations from this frequency, either higher or lower (including DC), resulted in diminished yields (Figure S14). Like **A3**, debromination was observed as a competitive side reaction for **A4**. Substrate **A5**, bearing a para electron-withdrawing $-CO_2Me$ substituent, displayed an oxidative addition rate comparable to **A1**, with f_{pred} = 0.14 Hz, yielding the highest amount of C−N coupled product (69%) at f_{exp} = 0.2 Hz. Again, frequencies above or below this value, including DC, led to reduced yields (Figure S15).

Altering the position of the $-CF_3$ group from *para* (**A1**) to *meta* (**A6**) resulted in a much slower oxidative addition process, with f_{pred} = 0.07 Hz. Experimental results corroborated this, with DC electrolysis providing the best yield for C−N coupling (87%) vs 71% with AC electrolysis at 0.2 Hz. For this substrate, no homocoupling product was detected, and only the starting material was not fully consumed (Figure S16). Substrate **A8** also demonstrated a slow oxidative addition rate, similar to **A7**, with both f_{pred} and f_{exp} indicating DC conditions as optimal for C−N coupling (46% yield, Figure S18). At 0.2 Hz, the C−N coupling yield is only 17%, with a significant amount of **A8** recovered (53%) because most of the Ni(II) catalyst only undergoes reversible and unproductive interconversion with its reduced Ni(I) form. Similarly, for **A9**, **A10**, and **A11**, their f_{pred} values fall between 0.06 and 0.1 Hz, consistent with the experimental observation that the DC conditions exhibit the highest yields (Figures S19−S21). Based on our observations, when the predicted optimal frequency was ≤0.1 Hz, the reaction showed the highest C−N coupling product selectivity in our home-built DC setup (interelectrode spacing ∼1 mm). Thus, a frequency of ∼0.1 Hz represents the critical value.

These results collectively underscore the robustness of the optimal frequency prediction method across a diverse range of aryl bromide substrates, highlighting the importance of electronic and steric factors in determining optimal electrochemical conditions for selective C−N bond formation.

CONCLUSIONS

In conclusion, we have demystified the AC-frequency-dependent C−N versus C−C selectivity in the Ni-catalyzed C−N cross-coupling reaction. Our results demonstrate that enhanced selectivity toward the C−N product at an optimal AC frequency arises from minimizing the exposure of a key intermediate, $Ni^{II}(Ar)Br$, which formed via oxidative addition between Ni^{I} and ArBr, to reducing conditions. Prolonged reduction favors the formation of an off-cycle Ni^{I} species that promotes undesired C−C homocoupling. Furthermore, we developed a convenient electroanalytical method based on cyclic voltammetry to accurately predict the optimal AC frequency across a range of substrates, eliminating the need for time-consuming trial-and-error optimization. This work also highlights the broader potential of AC waveforms to modulate the redox state of metal catalysts within catalytic cycles, thereby enabling control over reaction outcomes. Such strategies hold significant promise for advancing both synthetic and medicinal chemistry, where rapid and selective bond-forming transformations are critically important.

ASSOCIATED CONTENT

Supporting Information

The Supporting Information is available free of charge at https://pubs.acs.org/doi/10.1021/jacs.5c13155.

Details of experimental procedures, cyclicvoltammetry studies, determination of the optimal voltage and frequency foreach substrate, full characterization data, and copies of NMR spectra (PDF)

AUTHOR INFORMATION

Corresponding Author

Long Luo − *Department of Chemistry, University of Utah, Salt Lake City, Utah 84112, United States;* orcid.org/0000-0001-5771-6892; Email: long.luo@utah.edu

Authors

Atanu Hazra − *Department of Chemistry, University of Utah, Salt Lake City, Utah 84112, United States;* orcid.org/0000-0001-7625-3432

Marisa Organiscak − *Department of Chemistry, University of Utah, Salt Lake City, Utah 84112, United States;* orcid.org/0009-0008-7792-2624

Complete contact information is available at: https://pubs.acs.org/10.1021/jacs.5c13155

Author Contributions

The manuscript was written through the contributions of all authors.

Notes

The authors declare no competing financial interest.

ACKNOWLEDGMENTS

This work was primarily supported by NIH (1R35 GM142590). A.H., M.O., and L.L. also gratefully acknowledge support from the University of Utah and the Alfred P. Sloan Foundation (Grant # FH-2023-20829). ChatGPT was used to improve the language and clarity of the manuscript during its preparation.

REFERENCES

(1) Buskes, M. J.; Blanco, M. J. Impact of Cross-Coupling Reactions in Drug Discovery and Development. *Molecules* **2020**, *25* (15), 3493−3514.

(2) Parte, L. G.; Fernandez, S.; Sandonis, E.; Guerra, J.; Lopez, E. Transition-Metal-Catalyzed Transformations for the Synthesis of Marine Drugs. *Mar. Drugs* **2024**, *22* (6), 253.

(3) Biscoe, M. R.; Cornella, J.; Kalyani, D.; Neufeldt, S. From Established to Emerging: Evolution of Cross-Coupling Reactions. *J. Org. Chem.* **2024**, *89* (22), 16065−16069.

(4) Chen, A. R.; Yang, B.; Zhou, Z. H.; Zhu, F. Recent advances in transition-metal-catalyzed glycosyl cross-coupling reactions. *Chem. Catalysis* **2022**, *2* (12), 3430−3470.
(5) D'Alterio, M. C.; Casals-Cruanas, E.; Tzouras, N. V.; Talarico, G.; Nolan, S. P.; Poater, A. Mechanistic Aspects of the Palladium-Catalyzed Suzuki-Miyaura Cross-Coupling Reaction. *Chemistry* **2021**, *27* (54), 13481−13493.
(6) Biswas, S.; Weix, D. J. Mechanism and selectivity in nickel-catalyzed cross-electrophile coupling of aryl halides with alkyl halides. *J. Am. Chem. Soc.* **2013**, *135* (43), 16192−16197.
(7) Dawson, G. A.; Spielvogel, E. H.; Diao, T. Nickel-Catalyzed Radical Mechanisms: Informing Cross-Coupling for Synthesizing Non-Canonical Biomolecules. *Acc. Chem. Res.* **2023**, *56* (24), 3640−3653.
(8) Tsou, T. T.; Kochi, J. K. Mechanism of Oxidative Addition - Reaction of Nickel(0) Complexes with Aromatic Halides. *J. Am. Chem. Soc.* **1979**, *101* (21), 6319−6332.
(9) Feng, K.; Raguram, E. R.; Howard, J. R.; Peters, E.; Liu, C.; Sigman, M. S.; Buchwald, S. L. Development of a Deactivation-Resistant Dialkylbiarylphosphine Ligand for Pd-Catalyzed Arylation of Secondary Amines. *J. Am. Chem. Soc.* **2024**, *146* (39), 26609−26615.
(10) Liu, Y.; Sun, Y.; Deng, Y.; Qiu, Y. Electrochemical Amination of Aryl Halides with NH(3). *Angew. Chem., Int. Ed.* **2025**, *64* (24), No. e202504459.
(11) Raguram, E. R.; Dahl, J. C.; Jensen, K. F.; Buchwald, S. L. Kinetic Modeling Enables Understanding of Off-Cycle Processes in Pd-Catalyzed Amination of Five-Membered Heteroaryl Halides. *J. Am. Chem. Soc.* **2024**, *146* (48), 33035−33047.
(12) Beckers, I.; Vos, C.; Van Dessel, H.; Lauwers, A.; Stuyck, W.; Usoltsev, O.; Skorynina, A.; Bugaev, A.; De Vos, D. Overcoming Pd Catalyst Deactivation in the C-H Coupling of Tryptophan Residues in Water Using Air as the Oxidant. *ACS Catal.* **2024**, *14* (9), 7080−7086.
(13) Dziedzic, R. M.; Axtell, J. C.; Rheingold, A. L.; Spokoyny, A. M. Off-Cycle Processes in Pd-Catalyzed Cross-Coupling of Carboranes. *Org. Process Res. Dev.* **2019**, *23* (8), 1638−1645.
(14) Balcells, D.; Nova, A. Designing Pd and Ni Catalysts for Cross-Coupling Reactions by Minimizing Off-Cycle Species. *ACS Catal.* **2018**, *8* (4), 3499−3515.
(15) Ozkar, S.; Finke, R. G. Palladium(0) Nanoparticle Formation, Stabilization, and Mechanistic Studies: Pd(acac)(2) as a Preferred Precursor, [Bu(4)N](2)HPO(4) Stabilizer, plus the Stoichiometry, Kinetics, and Minimal, Four-Step Mechanism of the Palladium Nanoparticle Formation and Subsequent Agglomeration Reactions. *Langmuir* **2016**, *32* (15), 3699−3716.
(16) Li, M. B.; Backvall, J. E. Efficient Heterogeneous Palladium Catalysts in Oxidative Cascade Reactions. *Acc. Chem. Res.* **2021**, *54* (9), 2275−2286.
(17) Fantoni, T.; Palladino, C.; Grigolato, R.; Muzzi, B.; Ferrazzano, L.; Tolomelli, A.; Cabri, W. Mastering palladium-catalyzed cross-coupling reactions: the critical role of pre-catalyst reduction design. *Organic Chemistry Frontiers* **2025**, *12* (6), 1982−1991.
(18) Ruiz-Castillo, P.; Buchwald, S. L. Applications of Palladium-Catalyzed C-N Cross-Coupling Reactions. *Chem. Rev.* **2016**, *116* (19), 12564−12649.
(19) Zeng, L.; Yang, Q.; Wang, J.; Wang, X.; Wang, P.; Wang, S.; Lv, S.; Muhammad, S.; Liu, Y.; Yi, H.; et al. Programmed alternating current optimization of Cu-catalyzed C-H bond transformations. *Science* **2024**, *385* (6705), 216−223.
(20) Bortnikov, E. O.; Semenov, S. N. Coupling of Alternating Current to Transition-Metal Catalysis: Examples of Nickel-Catalyzed Cross-Coupling. *Journal of Organic Chemistry* **2021**, *86* (1), 782−793.
(21) De Bon, F.; Fantin, M.; Pereira, V. A.; Lourenco Bernardino, T. J.; Serra, A. C.; Matyjaszewski, K.; Coelho, J. F. J. Electrochemically Mediated Atom Transfer Radical Polymerization Driven by Alternating Current. *Angew. Chem., Int. Ed.* **2024**, *63* (29), No. e202406484.
(22) Till, N. A.; Oh, S.; MacMillan, D. W. C.; Bird, M. J. The Application of Pulse Radiolysis to the Study of Ni(I) Intermediates in Ni-Catalyzed Cross-Coupling Reactions. *J. Am. Chem. Soc.* **2021**, *143* (25), 9332−9337.
(23) Li, C.; Kawamata, Y.; Nakamura, H.; Vantourout, J. C.; Liu, Z.; Hou, Q.; Bao, D.; Starr, J. T.; Chen, J.; Yan, M.; et al. Electrochemically Enabled, Nickel-Catalyzed Amination. *Angew. Chem., Int. Ed.* **2017**, *56* (42), 13088−13093.
(24) Kawamata, Y.; Vantourout, J. C.; Hickey, D. P.; Bai, P.; Chen, L.; Hou, Q.; Qiao, W.; Barman, K.; Edwards, M. A.; Garrido-Castro, A. F.; et al. Electrochemically Driven, Ni-Catalyzed Aryl Amination: Scope, Mechanism, and Applications. *J. Am. Chem. Soc.* **2019**, *141* (15), 6392−6402.
(25) Luo, J.; Davenport, M. T.; Callister, C.; Minteer, S. D.; Ess, D. H.; Liu, T. L. Understanding Formation and Roles of Ni(II) Aryl Amido and Ni(III) Aryl Amido Intermediates in Ni-Catalyzed Electrochemical Aryl Amination Reactions. *J. Am. Chem. Soc.* **2023**, *145* (29), 16130−16141.
(26) Tang, T.; Hazra, A.; Min, D. S.; Williams, W. L.; Jones, E.; Doyle, A. G.; Sigman, M. S. Interrogating the Mechanistic Features of Ni(I)-Mediated Aryl Iodide Oxidative Addition Using Electroanalytical and Statistical Modeling Techniques. *J. Am. Chem. Soc.* **2023**, *145* (15), 8689−8699.
(27) Barman, K.; Edwards, M. A.; Hickey, D. P.; Sandford, C.; Qiu, Y.; Gao, R.; Minteer, S. D.; White, H. S. Electrochemical Reduction of [Ni(Mebpy)3]2+: Elucidation of the Redox Mechanism by Cyclic Voltammetry and Steady-State Voltammetry in Low Ionic Strength Solutions. *ChemElectroChem.* **2020**, *7* (6), 1473−1479.
(28) Qi, Y. Q.; Liu, S.; Xu, Y.; Li, Y.; Su, T.; Ni, H. L.; Gao, Y.; Yu, W.; Cao, P.; Hu, P.; et al. Nickel-Catalyzed Three-Component Cross-Electrophile Coupling of 1,3-Dienes with Aldehydes and Aryl Bromides. *Org. Lett.* **2022**, *24* (28), 5023−5028.
(29) Bard, A. J.; Faulkner, L. R. *Electrochemical methods: fundamentals and applications*; Wiley: New York, 1980.
(30) Everson, D. A.; Jones, B. A.; Weix, D. J. Replacing Conventional Carbon Nucleophiles with Electrophiles: Nickel-Catalyzed Reductive Alkylation of Aryl Bromides and Chlorides. *J. Am. Chem. Soc.* **2012**, *134* (14), 6146−6159.
(31) Romero-Arenas, A.; Popescu, M. V.; Goetz, M. K.; Bhatnagar, R.; Goljani, H.; Punchihewa, B. T.; Sanders, K. M.; Guzei, I. A.; Rafiee, M.; Weix, D. J.; et al. Reductively Induced Aryl Transmetalation: An Alternative Catalytically Relevant Ni-Catalyzed Biaryl Coupling Mechanism. *J. Am. Chem. Soc.* **2025**, *147* (25), 21697−21707.

https://doi.org/10.1021/jacs.5c13155
J. Am. Chem. Soc. XXXX, XXX, XXX−XXX